

Micromagnetic Simulations of Ferromagnetic Rings

Gabriel D. Chaves-O'Flynn, Ke Xiao, D.L. Stein, and A.D. Kent

Department of Physics, New York University, 4 Washington Place, New York, New York 10003, USA

(Dated: 09/12/07)

Thin nanomagnetic rings have generated interest for fundamental studies of magnetization reversal and also for their potential in various applications, particularly as magnetic memories. They are a rare example of a geometry in which an analytical solution for the rate of thermally induced magnetic reversal has been determined, in an approximation whose errors can be estimated and bounded. In this work, numerical simulations of soft ferromagnetic rings are used to explore aspects of the analytical solution. The evolution of the energy near the transition states confirms that, consistent with analytical predictions, thermally induced magnetization reversal can have one of two intermediate states: either constant or soliton-like saddle configurations, depending on ring size and externally applied magnetic field. The results confirm analytical predictions of a transition in thermally activated reversal behavior as magnetic field is varied at constant ring size. Simulations also show that the analytic one dimensional model continues to hold even for wide rings.

I. INTRODUCTION

The study of magnetization reversal in meso- and nanoscale ferromagnets is motivated by its importance in information storage applications. Ring-shaped thin film nanomagnets are particularly interesting because the absence of sharp edges inhibits nucleation which may precipitate undesired reversals. In addition, the geometry allows an analytic solution - rare in micromagnetics - for thermally induced reversal [1].

The lowest energy configurations of a soft ferromagnetic ring are a clockwise and counterclockwise circulation of the magnetization. The field generated by a current I flowing through the axis of the ring (\hat{z} -direction) will lift the degeneracy between the two orientations. For an effectively one-dimensional ring (ring width small compared to the average radius, so that external magnetic field strength within the ring is approximately constant), the reversal from the metastable state to the stable state can occur through either of two processes: a global rotation of the magnetization (which we will call the constant saddle state), or reversal initiated within a localized region and subsequent expansion (instanton saddle) [1]. Which of these processes occurs depends on both ring size and applied magnetic field. Using micromagnetic simulations in OOMMF [2] we have confirmed this general picture, even for more general two dimensional rings.

The model introduced in [1] predicted that the mag-

netization will be constrained to the film plane ($m_z = 0$) and the transition states will depend on both ring size and magnetic field. Important field and length scales in the problem are:

$$h = \frac{H_e}{H_c} = \frac{H_e}{\frac{\mu_0 M_s}{\pi} \left(\frac{t}{\Delta R} \right) \left| \ln \left(\frac{t}{R} \right) \right|} \quad (1)$$

$$l = \frac{R}{\lambda} \sqrt{2\pi \left(\frac{t}{\Delta R} \right) \left| \ln \left(\frac{t}{R} \right) \right|}. \quad (2)$$

Here M_s is the saturation magnetization, t is the ring thickness, ΔR is the ring width, R is the average radius, λ is the exchange length, H_e is the external magnetic field, and H_c is the field at which the metastable configuration becomes unstable. For $l \leq 2\pi\sqrt{1-h^2}$ the theory predicts a constant saddle, as shown in Fig. 1a, whereas for $l > 2\pi\sqrt{1-h^2}$, it predicts an instanton saddle (Figs. 1b, c). Both of these saddle configurations are described by a function $\phi_{h,l}(\theta)$ [1].

II. MICROMAGNETIC SIMULATIONS

We simulated the magnetization dynamics of rings of mean radius $R = 200$ nm and thickness $t = 2$ nm, for materials of exchange length λ ranging from 4 to 40 nm and constant saturation magnetization $M_s = 8 \times 10^5$ A/m (as in permalloy). The applied field has radial dependence $\vec{H}(r) = \frac{I}{2\pi r} \hat{\theta} = \frac{RH_e}{r} \hat{\theta}$, where H_e is the magnitude of the magnetic field generated by the current I at the mean radius of the annulus. We studied three different regimes for l : (1) $l < 2\pi$, where the transition state is predicted in [1] to be the constant saddle configuration (Fig. 1a); (2) l greater than but close to 2π and (3) $l \gg 2\pi$. The latter regime is relevant to recent experiments on nanomagnetic annuli [3, 4, 5, 6, 7, 8].

The magnitude of the exchange stiffness (and therefore exchange length) was varied so that l lay in all three regimes: respectively, $l = 6, 12$, and 60 . Two different ring widths were studied: $\Delta R = 40$ nm ($H_c = 73.9$ mT)

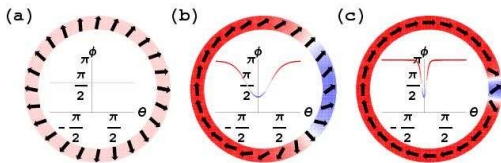


Figure 1: Magnetization configurations for $h = 0.2$. a) Constant saddle, b) Instanton Saddle at $l = 12$, c) Instanton saddle at $l = 60$.

and $\Delta R = 100$ nm ($H_c = 29.5$ mT). For different values of the parameter h the initial configurations (1a), (1b) and (1c) of the magnetization are allowed to evolve following the Landau-Lifshitz-Gilbert equations:

$$\frac{d\vec{M}}{dt} = -|\gamma|\vec{M} \times \vec{H}_{\text{eff}} - \frac{|\gamma|\alpha}{M_s}\vec{M} \times (\vec{M} \times H_{\text{eff}}) \quad (3)$$

where γ is the gyromagnetic ratio and H_{eff} is the effective magnetic field (i.e., including both the external field H_e and internal fields generated by the ring magnetization). The damping coefficient α can be set to one without loss of generality.

We first conducted tests to determine how well the analytical solution presented in [1] approximated the numerically determined two-dimensional saddle state in a narrow ring. We did this by initializing the spin configuration at time $t = 0$ using the instanton configuration given by Eqs. (8-11) of [1] with a fixed parameter h . We then allowed the system to evolve in time according to (3) with *different* values of the external field (of course, the external field is fixed during any particular run). A saddle state for a particular external field h_t must have the property that, for dynamics determined by slightly higher fields, the system falls to the stable state; for slightly lower fields, to the metastable state (or vice-versa). Therefore, for a fixed initial spin configuration defined by h we varied the field determining the dynamical evolution until a “transition field” h_t was found: for external fields less than h_t the system would evolve to the metastable configuration while for those greater than h_t it would evolve to the stable configuration. In this way the saddle configuration can be numerically determined. Values of h_t were obtained with a numerical uncertainty of $\delta h_t = 6 \times 10^{-3}$.

III. RESULTS AND DISCUSSION

The above discussion implies that the analytical solution is a good approximation to the actual configuration if the field h that determines the initial instanton configuration is close to the numerically determined h_t . The results are shown in Fig. 2, which shows the time evolution of the energy. Typically, after a short transient the system arrives at a configuration for which the energy stays almost constant in time before decaying to either of the stable states. As h gets closer to h_t , the system maintains a constant energy for longer times. We interpret this behavior as evidence that the analytically determined instanton predicted in [1] is indeed a close approximation to the actual saddle configuration. It can also be observed from Fig. 2 that at $h_t = 0.21$ the energy of the constant saddle is higher than that of the instanton saddle, as predicted in [1]. The slope of the curve during the subsequent relaxation depends on how fast the reversal propagates along the ring: as λ decreases the reversal time increases because both the domain wall width decreases and the effective circumference l increases. This

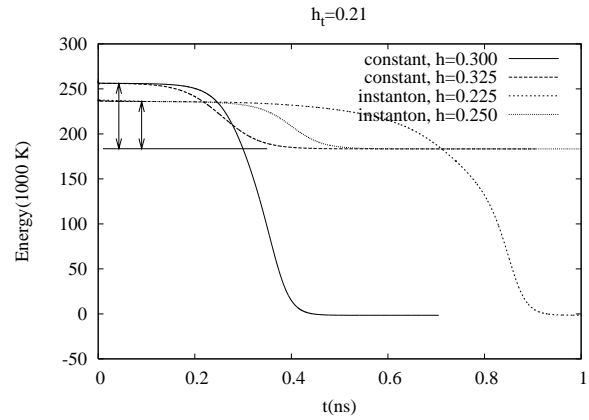


Figure 2: Time evolution of the total energy in a field $h_t = 0.21$, for the instanton ($h = \{0.225, 0.25\}$) and constant saddle configurations ($h = \{0.3, 0.325\}$) when $l=12$ and $\Delta R=40$ nm. These transition states are chosen to bracket the saddle state at the field of the simulation - the numerically determined h_t is not the same as the parameter h used to generate the saddle configurations from Eqs. (8-11) of [1] (see text for a fuller explanation). The arrows represent the magnitudes of the activation energy $\Delta E(h_t = 0.21)$ for each of the saddle states.

reduces the magnitude of the slope of the curve $E(t)$ during the reversal.

The reversal activation energy ΔE is summarized in Fig. 3 as a function of ΔR and λ . Every datum point corresponds to a step of $\Delta h = 0.1$ in the parameter of each of the saddle configurations. For fixed l , the energies of the instanton and saddle configurations cross at $h_c = \sqrt{1 - (\frac{2\pi}{l})^2}$; at higher fields the constant saddle is the lowest energy transition state. As predicted in [1], the instanton saddle has lower energy than the constant saddle for $h < h_c$, while for larger fields the constant saddle has a lower energy (Fig. 3a, $h = 0.57$). One should observe, however, that the predicted external switching field is larger than the numerically one. This is probably due to round-off from the simulations, but more importantly from the fact that the theoretical result is for a one-dimensional geometry whereas our simulations run in a (more realistic) two-dimensional mesh. So it's surprising that the agreement between the theoretical and numerically observed values for the switching field *improves* when the width ΔR is increased from 40 nm to 100 nm; cf. Figs. 3a-3c and 3b-3d. We believe this to be a consequence of the increased number of active cells in the simulation for the wider ring ($\Delta R = 100$ nm); it implies that the 1d solution is a good approximation even for fairly wide two-dimensional ring geometries.

The theory presented in [1] predicts that the difference between the activation energy of the constant saddle and the instanton saddle increases as λ decreases. This is also confirmed by our numerical simulations (compare Fig. 3a to 3b and 3c to 3d). This decrease is due to fact that the activation energy for the constant saddle

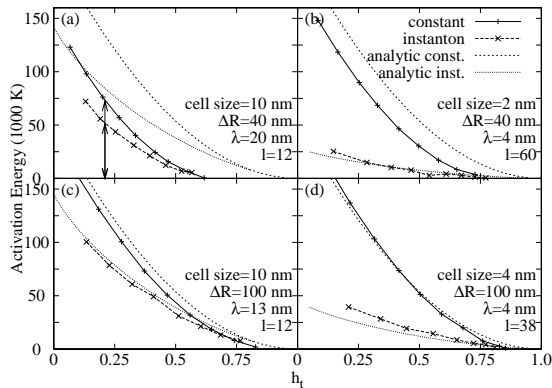


Figure 3: Energy barrier dependence on h_t for both saddle configurations in different regimes. Activation energies for $l = 12, \Delta R = 40$ nm at $h_t = 0.21$ are shown for comparison with Fig. 1. Data points represent $h = \{0.1, \dots, 0.9\}$. For comparison, theoretical lines are plotted for the activation energy. The crossing of the analytical curves in (b) and (d) is not visible due to the graphical resolution.

is independent of λ while the activation energy for the instanton (whose size is order λ) is roughly proportional to λ . This latter dependence of activation energy on λ is in turn understood by observing that the total energy of the ring is the result of three contributions: Zeeman, exchange and magnetostatic energy. The constant saddle, metastable and stable states all have the same exchange energy, so the exchange energy does not contribute to the energy barrier of the constant saddle. Both remaining terms (magnetostatic and Zeeman energy) are independent of λ , so the constant saddle activation energy does not change with λ . On the other hand, in most of

the ring, the metastable and instanton configurations are almost identical, so that their energy difference is the result of a fluctuation in a small region of the ring, whose size is of order λ . The barrier (both theoretical and experimental) for the instanton saddle is therefore smaller in Figs. 3b and 3d than in Figs. 3a and 3c.

IV. CONCLUSION

In these studies we have conducted numerical micro-magnetic simulations of the transition states for magnetization reversal in thin annular nanomagnets to test the theory presented in [1]. Numerical calculations are consistent with the prediction that in the parameter space defined by (h, l) there is a region for which a non-constant, soliton-like transition state (the “instanton” state) exists and has lower energy than the constant transition state. An important assumption made in [1] is that the magnetostatic contribution is dominated by the surface magnetostatic effect. This is supported by the above simulations. One would expect that by increasing the ring width the bulk magnetostatic energy would increase in magnitude and eventually become nonnegligible, so that other transitions paths become more probable (e.g., vortex-like states). This should eventually occur; however, up to the appreciable $\Delta R/R$ values studied here, the approximations made in [1] remain valid.

This research is supported in part by U.S. National Science Foundation Grants DMR-0706322 (ADK), DMS-0601179 and 0651077 (DLS), and an NYU Research Challenge Fund award.

-
- [1] K. Martens, D.L. Stein and A.D. Kent, Phys. Rev. B **73**, 054413 (2006).
 - [2] M. J. Donahue and D. G. Porter, OOMMF User's Guide, Version 1.0, Interagency Report NISTIR 6376, National Institute of Standards and Technology, Gaithersburg, MD (Sept 1999). <http://math.nist.gov/oommf/>
 - [3] T. Yang, M. Hara, A. Hirohata, T. Kimura and Y. Otani, Appl. Phys. Lett. **90**, 022504 (2007).
 - [4] F.J. Castaño, C. A. Ross, C. Frandsen, A. Eilez, D. Gil, H. Smith, M. Redjal, and F.B. Humphrey. Phys. Rev. B **67**, 184425 (2003).
 - [5] F.J. Castaño, D. Morecroft, and C. A. Ross, Phys Rev B **74**, 224401 (2006).
 - [6] Matthew T. Moneck and Jian-Gang Zhu, J. Appl. Phys. **99** 08H709 (2006).
 - [7] J. Rothman, M. Kläui, L. Lopez-Diaz, C.A.F. Vaz, A. Bleloch, J.A.C. Bland, Z. Cui and R. Speaks, Phys. Rev. Lett. **86**, 1098 (2001).
 - [8] Jian-Gang Zhu, Youfeng Zheng and Gary A. Prinz, J. Appl. Phys. **87**, 6668 (2000).